

Sensorless position estimation of Permanent-Magnet Synchronous Motors using a saturation model

Al Kassem Jebai, François Malrait, Philippe Martin and Pierre Rouchon

Abstract—Sensorless control of Permanent-Magnet Synchronous Motors (PMSM) at low velocity remains a challenging task. A now well-established method consists in injecting a high-frequency signal and use the rotor saliency, both geometric and magnetic-saturation induced. This paper proposes a clear and original analysis based on second-order averaging of how to recover the position information from signal injection; this analysis blends well with a general model of magnetic saturation. It also proposes a simple parametric model of the saturated PMSM, based on an energy function which simply encompasses saturation and cross-saturation effects. Experimental results on a surface-mounted PMSM and an interior magnet PMSM illustrate the relevance of the approach.

Index Terms—Permanent-magnet synchronous motor, sensorless position estimation, signal injection, magnetic saturation, energy-based modeling, averaging.

I. INTRODUCTION

PERMANENT-Magnet Synchronous Motors (PMSM) are widely used in industry. In the so-called “sensorless” mode of operation, the rotor position and velocity are not measured and the control law must make do with only current measurements. While sensorless control at medium to high velocities is well understood, with many reported control schemes and industrial products, sensorless control at low velocity remains a challenging task. The reason is that observability degenerates at zero velocity, causing a serious problem in the necessary rotor position estimation.

A now well-established method to overcome this problem is to add some persistent excitation by injecting a high-frequency signal [1] and use the rotor saliency, whether geometric for Interior Permanent-Magnet machines or induced by main flux saturation for Surface Permanent-Magnet machines [2]–[10]. Signal injection is moreover considered as a standard building block in hybrid control schemes for complete drives operating from zero to full speed [11]–[15].

However to get a good position estimation under high-load condition it is important to take cross-saturation into account [16]–[26]. It is thus necessary to rely on a model of the saturated PMSM adapted to control purposes, i.e. rich enough to capture in particular cross-saturation but also simple enough to be used in real-time and to be easily identified in the field; see [27]–[32] for references more or less in this spirit.

The contribution of this paper, which builds on the preliminary work [33], is twofold: on the one hand it proposes a clear

and original analysis based on second-order averaging of how to recover the position information from signal injection; this analysis can accommodate to any form of injected signals, e.g. square signals as in [34], and blends well with a general model of magnetic saturation including cross-saturation. On the other hand a simple parametric model of the saturated PMSM, well-adapted to control purposes, is introduced; it is based on an energy function which simply encompasses saturation and cross-saturation effects.

The paper runs as follows: section II presents the saturation model. In section III position estimation by signal injection is studied thanks to second-order averaging. Section IV is devoted to the estimation of the parameters entering the saturation model using once again signal injection and averaging. Finally section IV-C experimentally demonstrates on two kinds of motors (with interior magnets and surface-mounted magnets) the relevance of the approach and the necessity of considering saturation to correctly estimate the position.

II. AN ENERGY-BASED MODEL OF THE SATURATED PMSM

A. Notations

In the sequel we denote by $x_{ij} := (x_i, x_j)^T$ the vector made from the real numbers x_i and x_j , where ij can be dq , $\alpha\beta$ or $\gamma\delta$. We also define the matrices

$$M_\mu := \begin{pmatrix} \cos \mu & -\sin \mu \\ \sin \mu & \cos \mu \end{pmatrix} \quad \text{and} \quad \mathcal{K} := \begin{pmatrix} 0 & -1 \\ 1 & 0 \end{pmatrix},$$

and we have the useful relation

$$\frac{dM_\mu}{d\mu} = \mathcal{K}M_\mu = M_\mu\mathcal{K}.$$

B. Energy-based model

The model of a two-axis PMSM expressed in the synchronous $d-q$ frame reads

$$\frac{d\phi_{dq}}{dt} = u_{dq} - Ri_{dq} - \omega\mathcal{K}(\phi_{dq} + \phi_m) \quad (1)$$

$$\frac{J}{n^2} \frac{d\omega}{dt} = \frac{3}{2} i_{dq}^T \mathcal{K}(\phi_{dq} + \phi_m) - \frac{\tau_L}{n} \quad (2)$$

$$\frac{d\theta}{dt} = \omega, \quad (3)$$

with ϕ_{dq} flux linkage due to the current; $\phi_m := (\lambda, 0)^T$ constant flux linkage due to the permanent magnet; u_{dq} impressed voltage and i_{dq} stator current; ω and θ rotor (electrical) speed and position; R stator resistance; n number of pole pairs; J inertia moment and τ_L load torque. The physically impressed voltages are $u_{\alpha\beta} := M_\theta u_{dq}$ while the physically measurable

A-K. Jebai, P. Martin and P. Rouchon are with the Centre Automatique et Systèmes, MINES ParisTech, 75006 Paris, France {al-kassem.jebai, philippe.martin, pierre.rouchon}@mines-paristech.fr

F. Malrait is with Schneider Toshiba Inverter Europe, 27120 Pacy-sur-Eure, France francois.malrait@schneider-electric.com

currents are $i_{\alpha\beta} := M_\theta i_{dq}$. The current can be expressed in function of the flux linkage thanks to a suitable energy function $\mathcal{H}(\phi_d, \phi_q)$ by

$$i_{dq} = \mathcal{I}_{dq}(\phi_{dq}) := \begin{pmatrix} \partial_1 \mathcal{H}(\phi_d, \phi_q) \\ \partial_2 \mathcal{H}(\phi_d, \phi_q) \end{pmatrix}, \quad (4)$$

where $\partial_k \mathcal{H}$ denotes the partial derivative w.r.t. the k^{th} variable [35], [36]; without loss of generality $\mathcal{H}(0,0) = 0$. Such a relation between flux linkage and current naturally encompasses cross-saturation effects.

For an unsaturated PMSM this energy function reads

$$\mathcal{H}_l(\phi_d, \phi_q) = \frac{1}{2L_d} \phi_d^2 + \frac{1}{2L_q} \phi_q^2$$

where L_d and L_q are the motor self-inductances, and we recover the usual linear relations

$$\begin{aligned} i_d &= \partial_1 \mathcal{H}_l(\phi_d, \phi_q) = \frac{\phi_d}{L_d} \\ i_q &= \partial_2 \mathcal{H}_l(\phi_d, \phi_q) = \frac{\phi_q}{L_q}. \end{aligned}$$

Notice the expression for \mathcal{H} should respect the symmetry of the PMSM w.r.t the direct axis, i.e.

$$\mathcal{H}(\phi_d, -\phi_q) = \mathcal{H}(\phi_d, \phi_q), \quad (5)$$

which is obviously the case for \mathcal{H}_l . Indeed (1)–(3) is left unchanged by the transformation

$$\begin{aligned} (u_d, u_q, \phi_d, \phi_q, i_d, i_q, \omega, \theta, \tau_L) &\rightarrow \\ (u_d, -u_q, \phi_d, -\phi_q, i_d, -i_q, -\omega, -\theta, -\tau_L). \end{aligned}$$

C. Parametric description of magnetic saturation

Magnetic saturation can be accounted for by considering a more complicated magnetic energy function \mathcal{H} , having \mathcal{H}_l for quadratic part but including also higher-order terms. From experiments saturation effects are well captured by considering only third- and fourth-order terms, hence

$$\begin{aligned} \mathcal{H}(\phi_d, \phi_q) &= \mathcal{H}_l(\phi_d, \phi_q) \\ &+ \sum_{i=0}^3 \alpha_{3-i,i} \phi_d^{3-i} \phi_q^i + \sum_{i=0}^4 \alpha_{4-i,i} \phi_d^{4-i} \phi_q^i. \end{aligned}$$

This is a perturbative model where the higher-order terms appear as corrections of the dominant term \mathcal{H}_l . The nine coefficients α_{ij} together with L_d, L_q are motor dependent. But (5) implies $\alpha_{2,1} = \alpha_{0,3} = \alpha_{3,1} = \alpha_{1,3} = 0$, so that the energy function eventually reads

$$\begin{aligned} \mathcal{H}(\phi_d, \phi_q) &= \mathcal{H}_l(\phi_d, \phi_q) + \alpha_{3,0} \phi_d^3 + \alpha_{1,2} \phi_d \phi_q^2 \\ &+ \alpha_{4,0} \phi_d^4 + \alpha_{2,2} \phi_d^2 \phi_q^2 + \alpha_{0,4} \phi_q^4. \end{aligned} \quad (6)$$

From (4) and (6) the currents are then explicitly given by

$$i_d = \frac{\phi_d}{L_d} + 3\alpha_{3,0} \phi_d^2 + \alpha_{1,2} \phi_q^2 + 4\alpha_{4,0} \phi_d^3 + 2\alpha_{2,2} \phi_d \phi_q^2 \quad (7)$$

$$i_q = \frac{\phi_q}{L_q} + 2\alpha_{1,2} \phi_d \phi_q + 2\alpha_{2,2} \phi_d^2 \phi_q + 4\alpha_{0,4} \phi_q^3, \quad (8)$$

which are the so-called flux-current magnetization curves.

To conclude, the model of the saturated PMSM is given by (1)–(3) and (7)–(8), with $\phi_d, \phi_q, \omega, \theta$ as state variables. The magnetic saturation effects are represented by the five parameters $\alpha_{3,0}, \alpha_{1,2}, \alpha_{4,0}, \alpha_{2,2}, \alpha_{0,4}$.

D. Model with i_d, i_q as state variables

The model of the PMSM is usually expressed with currents as state variables. This can be achieved here by time differentiating $i_{dq} = \mathcal{I}_{dq}(\phi_{dq})$,

$$\frac{di_{dq}}{dt} = D\mathcal{I}_{dq}(\phi_{dq}) \frac{d\phi_{dq}}{dt},$$

with $\frac{d\phi_{dq}}{dt}$ given by (1). Fluxes are then expressed as $\phi_{dq} = \mathcal{I}_{dq}^{-1}(i_{dq})$ by inverting the nonlinear relations (7)–(8); rather than performing the exact inversion, we can take advantage of the fact the coefficients $\alpha_{i,j}$ are experimentally small. At first order w.r.t. the $\alpha_{i,j}$ we have $\phi_d = L_d i_d + \mathcal{O}(|\alpha_{i,j}|)$ and $\phi_q = L_q i_q + \mathcal{O}(|\alpha_{i,j}|)$; plugging these expressions into (7)–(8) and neglecting $\mathcal{O}(|\alpha_{i,j}|^2)$ terms, we easily find

$$\begin{aligned} \phi_d &= L_d (i_d - 3\alpha_{3,0} L_d^2 i_d^2 - \alpha_{1,2} L_q^2 i_q^2 \\ &\quad - 4\alpha_{4,0} L_d^3 i_d^3 - 2\alpha_{2,2} L_d L_q^2 i_d i_q^2) \end{aligned} \quad (9)$$

$$\begin{aligned} \phi_q &= L_q (i_q - 2\alpha_{1,2} L_d L_q i_d i_q - \\ &\quad 2\alpha_{2,2} L_d^2 L_q i_d^2 i_q - 4\alpha_{0,4} L_q^3 i_q^3). \end{aligned} \quad (10)$$

Notice the matrix

$$\begin{pmatrix} G_{dd}(i_{dq}) & G_{dq}(i_{dq}) \\ G_{dq}(i_{dq}) & G_{qq}(i_{dq}) \end{pmatrix} := D\mathcal{I}_{dq}(\mathcal{I}_{dq}^{-1}(i_{dq})), \quad (11)$$

with coefficients easily found to be

$$G_{dd}(i_{dq}) = \frac{1}{L_d} + 6\alpha_{3,0} L_d i_d + 12\alpha_{4,0} L_d^2 i_d^2 + 2\alpha_{2,2} L_q^2 i_q^2$$

$$G_{dq}(i_{dq}) = 2\alpha_{1,2} L_q i_q + 4\alpha_{2,2} L_d i_d L_q i_q$$

$$G_{qq}(i_{dq}) = \frac{1}{L_q} + 2\alpha_{1,2} L_d i_d + 2\alpha_{2,2} L_d^2 i_d^2 + 12\alpha_{0,4} L_q^2 i_q^2,$$

is by construction symmetric; indeed

$$D\mathcal{I}_{dq}(\phi_{dq}) = \begin{pmatrix} \partial_{11} \mathcal{H}(\phi_d, \phi_q) & \partial_{21} \mathcal{H}(\phi_d, \phi_q) \\ \partial_{12} \mathcal{H}(\phi_d, \phi_q) & \partial_{22} \mathcal{H}(\phi_d, \phi_q) \end{pmatrix}$$

and $\partial_{12} \mathcal{H} = \partial_{21} \mathcal{H}$. Therefore the inductance matrix

$$\begin{pmatrix} L_{dd}(i_{dq}) & L_{dq}(i_{dq}) \\ L_{dq}(i_{dq}) & L_{qq}(i_{dq}) \end{pmatrix} := \begin{pmatrix} G_{dd}(i_{dq}) & G_{dq}(i_{dq}) \\ G_{dq}(i_{dq}) & G_{qq}(i_{dq}) \end{pmatrix}^{-1}.$$

is also symmetric, though this is not always acknowledged in saturation models encountered in the literature.

III. POSITION ESTIMATION BY HIGH FREQUENCY VOLTAGE INJECTION

A. Signal injection and averaging

A general sensorless control law can be expressed as

$$u_{\alpha\beta} = M_{\theta_c} u_{\gamma\delta} \quad (12)$$

$$\frac{d\theta_c}{dt} = \omega_c \quad (13)$$

$$\frac{d\eta}{dt} = a(M_{\theta_c} i_{\gamma\delta}, \theta_c, \eta, t) \quad (14)$$

$$\omega_c = \Omega_c(M_{\theta_c} i_{\gamma\delta}, \theta_c, \eta, t) \quad (15)$$

$$u_{\gamma\delta} = \mathcal{U}_{\gamma\delta}(M_{\theta_c} i_{\gamma\delta}, \theta_c, \eta, t), \quad (16)$$

where the measured currents $i_{\alpha\beta} = M_{\theta_c} i_{\gamma\delta}$ are used to compute $u_{\gamma\delta}$, ω_c and the evolution of the internal (vector) variable η of the controller; θ_c and ω_c are known by design.

It will be convenient to write the system equations (1)–(3) in the $\gamma - \delta$ frame defined by $x_{\gamma\delta} := M_{\theta - \theta_c} x_{dq}$, which gives

$$\frac{d\phi_{\gamma\delta}}{dt} = u_{\gamma\delta} - R i_{\gamma\delta} - \omega_c \mathcal{K} \phi_{\gamma\delta} - \omega \mathcal{K} M_{\theta - \theta_c} \phi_m \quad (17)$$

$$\frac{J}{n^2} \frac{d\omega}{dt} = \frac{3}{2} i_{\gamma\delta}^T \mathcal{K} (\phi_{\gamma\delta} + M_{\theta - \theta_c} \phi_m) - \frac{\tau_L}{n} \quad (18)$$

$$\frac{d\theta}{dt} = \omega, \quad (19)$$

where from (7)–(8) currents and fluxes are related by

$$i_{\gamma\delta} = M_{\theta - \theta_c} \mathcal{I}_{dq} (M_{\theta - \theta_c}^T \phi_{\gamma\delta}). \quad (20)$$

To estimate the position we will superimpose on some desirable control law (16) a fast-varying pulsating voltage,

$$u_{\gamma\delta} = \mathcal{U}_{\gamma\delta} (M_{\theta_c} i_{\gamma\delta}, \theta_c, \eta, t) + \tilde{u}_{\gamma\delta} f(\Omega t), \quad (21)$$

where f is a 2π -periodic function with zero mean and $\tilde{u}_{\gamma\delta}$ could like $\mathcal{U}_{\gamma\delta}$ depend on $M_{\theta_c} i_{\gamma\delta}, \theta_c, \eta, t$ (though it is always taken constant in the sequel). The constant pulsation Ω is chosen “large”, so that $f(\Omega t)$ can be seen as a “fast” oscillation; typically $\Omega := 2\pi \times 500$ rad/s in the experiments in section IV-C.

If we apply this modified control law to (17)–(19), then it can be shown the solution of the closed loop system is

$$\phi_{\gamma\delta} = \bar{\phi}_{\gamma\delta} + \frac{\tilde{u}_{\gamma\delta}}{\Omega} F(\Omega t) + \mathcal{O}\left(\frac{1}{\Omega^2}\right) \quad (22)$$

$$\omega = \bar{\omega} + \mathcal{O}\left(\frac{1}{\Omega^2}\right) \quad (23)$$

$$\theta = \bar{\theta} + \mathcal{O}\left(\frac{1}{\Omega^2}\right) \quad (24)$$

$$\theta_c = \bar{\theta}_c + \mathcal{O}\left(\frac{1}{\Omega^2}\right) \quad (25)$$

$$\eta = \bar{\eta} + \mathcal{O}\left(\frac{1}{\Omega^2}\right), \quad (26)$$

where F is the primitive of f with zero mean (F clearly has the same period as f); $(\bar{\phi}_{\gamma\delta}, \bar{\omega}, \bar{\theta}, \bar{\theta}_c, \bar{\eta})$ is the “slowly-varying” component of $(\phi_{\gamma\delta}, \omega, \theta, \theta_c, \eta)$, i.e. satisfies

$$\frac{d\bar{\phi}_{\gamma\delta}}{dt} = \bar{u}_{\gamma\delta} - R \bar{i}_{\gamma\delta} - \bar{\omega}_c \mathcal{K} \bar{\phi}_{\gamma\delta} - \omega \mathcal{K} M_{\bar{\theta} - \bar{\theta}_c} \phi_m$$

$$\frac{J}{n^2} \frac{d\bar{\omega}}{dt} = \frac{3}{2} \bar{i}_{\gamma\delta}^T \mathcal{K} (\bar{\phi}_{\gamma\delta} + M_{\bar{\theta} - \bar{\theta}_c} \phi_m) - \frac{\tau_L}{n}$$

$$\frac{d\bar{\theta}}{dt} = \bar{\omega}$$

$$\frac{d\bar{\theta}_c}{dt} = \bar{\omega}_c$$

$$\frac{d\bar{\eta}}{dt} = a(M_{\bar{\theta}_c} \bar{i}_{\gamma\delta}, \bar{\theta}_c, \bar{\eta}, t),$$

where

$$\bar{i}_{\gamma\delta} = M_{\bar{\theta} - \bar{\theta}_c} \mathcal{I}_{dq} (M_{\bar{\theta} - \bar{\theta}_c}^T \bar{\phi}_{\gamma\delta}) \quad (27)$$

$$\bar{\omega}_c = \Omega_c (M_{\bar{\theta}_c} \bar{i}_{\gamma\delta}, \bar{\theta}_c, \bar{\eta}, t)$$

$$\bar{u}_{\gamma\delta} = \mathcal{U}_{\gamma\delta} (M_{\bar{\theta}_c} \bar{i}_{\gamma\delta}, \bar{\theta}_c, \bar{\eta}, t).$$

Notice this slowly-varying system is exactly the same as (17)–(19) acted upon by the unmodified control law (12)–(16). In other words adding signal injection:

- has a very small effect of order $\mathcal{O}\left(\frac{1}{\Omega^2}\right)$ on the mechanical variables θ, ω and the controller variables θ_c, η
- has a small effect of order $\mathcal{O}\left(\frac{1}{\Omega}\right)$ on the flux $\phi_{\gamma\delta}$; this effect will be used in the next section to extract the position information from the measured currents.

The proof relies on a direct application of second-order averaging of differential equations, see [37] section 2.9.1 and for the slow-time dependence section 3.3. Indeed setting $\varepsilon := \frac{1}{\Omega}$, $\sigma := \frac{t}{\varepsilon}$, and $x := (\phi_{\gamma\delta}, \omega, \theta, \theta_c, \eta)$, (17)–(19) acted upon by the modified control law (12)–(15) and (21) is in the so-called standard form for averaging (with slow-time dependence)

$$\frac{dx}{d\sigma} = \varepsilon f_1(x, \varepsilon\sigma, \sigma) := \varepsilon (\bar{f}_1(x, \varepsilon\sigma) + \tilde{f}_1(x, \varepsilon\sigma) f(\sigma)),$$

with f_1 T -periodic w.r.t. its third variable ($T = 2\pi$ in our case) and ε as a small parameter. Therefore its solution can be approximated as

$$x(\sigma) = z(\sigma) + \varepsilon (u_1(z(\sigma), \varepsilon\sigma, \sigma) + \mathcal{O}(\varepsilon^2)),$$

where $z(\sigma)$ is the solution of

$$\frac{dz}{d\sigma} = \varepsilon g_1(z, \varepsilon\sigma) + \varepsilon^2 g_2(z, \varepsilon\sigma)$$

and

$$g_1(y, \varepsilon\sigma) := \frac{1}{T} \int_0^T f_1(y, \varepsilon\sigma, s) ds = \bar{f}_1(y, \varepsilon\sigma)$$

$$\begin{aligned} v_1(y, \varepsilon\sigma, \sigma) &:= \int_0^\sigma (f_1(y, \varepsilon\sigma, s) - g_1(y, \varepsilon\sigma)) ds \\ &= \tilde{f}_1(y, \varepsilon\sigma) \int_0^\sigma f(s) ds \end{aligned}$$

$$\begin{aligned} u_1(y, \varepsilon\sigma, \sigma) &:= v_1(y, \varepsilon\sigma, \sigma) - \frac{1}{T} \int_0^T v_1(y, \varepsilon\sigma, s) ds \\ &= \tilde{f}_1(y, \varepsilon\sigma) F(\sigma) \end{aligned}$$

$$\begin{aligned} K_2(y, \varepsilon\sigma, \sigma) &:= \partial_1 f_1(y, \varepsilon\sigma, \sigma) u_1(y, \varepsilon\sigma, \sigma) \\ &\quad - \partial_1 u_1(y, \varepsilon\sigma, \sigma) g_1(y, \varepsilon\sigma) \\ &= [\bar{f}_1, \tilde{f}_1](y, \varepsilon\sigma) F(\sigma) \\ &\quad + \frac{1}{2} \partial_1 \tilde{f}_1(y, \varepsilon\sigma) \tilde{f}_1(y, \varepsilon\sigma) \frac{dF^2(\sigma)}{d\sigma} \end{aligned}$$

$$g_2(y, \varepsilon\sigma) := \frac{1}{T} \int_0^T K_2(y, \varepsilon\sigma, s) ds = 0.$$

We have set

$$[\bar{f}_1, \tilde{f}_1](y, \varepsilon\sigma) := \partial_1 \bar{f}_1(y, \varepsilon\sigma) \tilde{f}_1(y, \varepsilon\sigma) - \partial_1 \tilde{f}_1(y, \varepsilon\sigma) \bar{f}_1(y, \varepsilon\sigma)$$

and $F(\sigma) := \int_0^\sigma f(s) ds - \frac{1}{T} \int_0^T \int_0^\sigma f(s) ds d\sigma$, i.e. F is the (of course T -periodic) primitive of f with zero mean.

Translating back to the original variables eventually yields the desired result (22)–(26).

B. Position estimation

We now express the effect of signal injection on the currents: plugging (22) into (20) we have

$$\begin{aligned} i_{\gamma\delta} &= M_{\bar{\theta}-\bar{\theta}_c+\mathcal{O}(\frac{1}{\Omega^2})} \\ &\mathcal{I}_{dq}\left(M_{\bar{\theta}-\bar{\theta}_c+\mathcal{O}(\frac{1}{\Omega^2})}^T(\bar{\phi}_{\gamma\delta} + \frac{\tilde{u}_{\gamma\delta}}{\Omega}F(\Omega t) + \mathcal{O}(\frac{1}{\Omega^2}))\right) \\ &= \bar{i}_{\gamma\delta} + \tilde{i}_{\gamma\delta}F(\Omega t) + \mathcal{O}(\frac{1}{\Omega^2}), \end{aligned} \quad (28)$$

where we have used (27) and performed a first-order expansion to get

$$\begin{aligned} \tilde{i}_{\gamma\delta} &:= M_{\bar{\theta}-\bar{\theta}_c}^T D\mathcal{I}_{dq}\left(M_{\bar{\theta}-\bar{\theta}_c}^T \bar{\phi}_{\gamma\delta}\right) M_{\bar{\theta}-\bar{\theta}_c}^T \frac{\tilde{u}_{\gamma\delta}}{\Omega} \\ &= M_{\bar{\theta}-\bar{\theta}_c}^T D\mathcal{I}_{dq}\left(\mathcal{I}_{dq}^{-1}\left(M_{\bar{\theta}-\bar{\theta}_c}^T \bar{i}_{\gamma\delta}\right)\right) M_{\bar{\theta}-\bar{\theta}_c}^T \frac{\tilde{u}_{\gamma\delta}}{\Omega}. \end{aligned} \quad (29)$$

We will see in the next section how to recover $\tilde{i}_{\gamma\delta}$ and $\bar{i}_{\gamma\delta}$ from the measured currents $i_{\gamma\delta}$. Therefore (29) gives two (redundant) relations relating the unknown angle $\bar{\theta}$ to the known variables $\bar{\theta}_c, \tilde{i}_{dq}, \bar{i}_{\gamma\delta}, \tilde{u}_{dq}$, provided the matrix

$$\mathcal{S}(\mu, \bar{i}_{\gamma\delta}) := M_{\mu} D\mathcal{I}_{dq}\left(\mathcal{I}_{dq}^{-1}\left(M_{\mu}^T \bar{i}_{\gamma\delta}\right)\right) M_{\mu}^T$$

effectively depends on its first argument μ . This ‘‘saliency condition’’ is what is needed to ensure nonlinear observability. The explicit expression for $\mathcal{S}(\mu, \bar{i}_{\gamma\delta})$ is obtained thanks to (11). In the case of an unsaturated magnetic circuit this matrix boils down to

$$\begin{aligned} \mathcal{S}(\mu, \bar{i}_{\gamma\delta}) &= M_{\mu} \begin{pmatrix} \frac{1}{L_d} & 0 \\ 0 & \frac{1}{L_q} \end{pmatrix} M_{\mu}^T \\ &= \frac{L_d+L_q}{2L_dL_q} \begin{pmatrix} 1 + \frac{L_d-L_q}{L_d+L_q} \cos 2\mu & \frac{L_d-L_q}{L_d+L_q} \sin 2\mu \\ \frac{L_d-L_q}{L_d+L_q} \sin 2\mu & 1 - \frac{L_d-L_q}{L_d+L_q} \cos 2\mu \end{pmatrix} \end{aligned}$$

and does not depend on $i_{\gamma\delta}$; notice this matrix does not depend on μ for an unsaturated machine with no geometric saliency. Notice also (29) defines in that case two solutions on $]-\pi, \pi]$ for the angle $\bar{\theta}$ since $\mathcal{S}(\mu, \bar{i}_{\gamma\delta})$ is actually a function of 2μ ; in the saturated case there is generically only one solution, except for some particular values of $\bar{i}_{\gamma\delta}$.

There are several ways to extract the rotor angle information from (29), especially for real-time use inside a feedback law. In this paper we just want to demonstrate the validity of (29) and we will be content with directly solving it through a nonlinear least square problem; in other words we estimate the rotor position as

$$\hat{\theta} = \theta_c + \arg \min_{\mu \in]-\pi, \pi]} \left\| \tilde{i}_{\gamma\delta} - \mathcal{S}(\mu, \bar{i}_{\gamma\delta}) \frac{\tilde{u}_{\gamma\delta}}{\Omega} \right\|^2. \quad (30)$$

C. Current demodulation

To estimate the position information using e.g. (30) it is necessary to extract the low- and high-frequency components $\bar{i}_{\gamma\delta}$ and $\tilde{i}_{\gamma\delta}$ from the measured current $i_{\gamma\delta}$. Since by (28) $i_{\gamma\delta}(t) \approx \bar{i}_{\gamma\delta}(t) + \tilde{i}_{\gamma\delta}(t)F(\Omega t)$ with $\bar{i}_{\gamma\delta}$ and $\tilde{i}_{\gamma\delta}$ by construction

nearly constant on one period of F , we may write

$$\begin{aligned} \bar{i}_{\gamma\delta}(t) &\approx \frac{1}{T} \int_{t-T}^t i_{\gamma\delta}(s) ds \\ \tilde{i}_{\gamma\delta}(t) &\approx \frac{\int_{t-T}^t i_{\gamma\delta}(s) F(\Omega s) ds}{\int_0^T F^2(\Omega s) ds}, \end{aligned}$$

where $T := \frac{2\pi}{\Omega}$. Indeed as F is 2π -periodic with zero mean,

$$\begin{aligned} \int_{t-T}^t i_{\gamma\delta}(s) ds &\approx \bar{i}_{\gamma\delta}(t) \int_{t-T}^t ds + \tilde{i}_{\gamma\delta}(t) \int_{t-T}^t F(\Omega s) ds \\ &= T\bar{i}_{\gamma\delta}(t) \\ \int_{t-T}^t i_{\gamma\delta}(s) F(\Omega s) ds &\approx \bar{i}_{\gamma\delta}(t) \int_{t-T}^t F(\Omega s) ds \\ &\quad + \tilde{i}_{\gamma\delta}(t) \int_{t-T}^t F^2(\Omega s) ds \\ &= \tilde{i}_{\gamma\delta}(t) \int_0^T F^2(\Omega s) ds. \end{aligned}$$

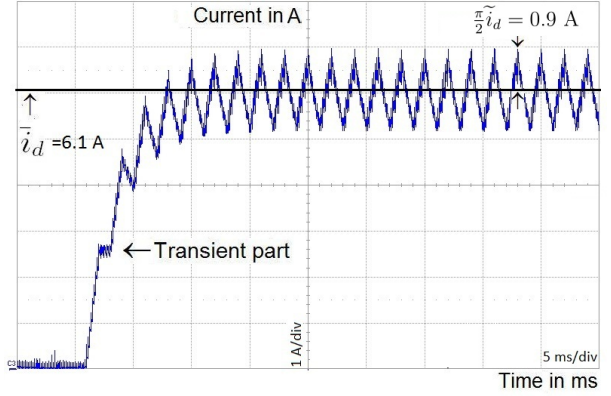


Fig. 1. Experimental time response of i_d in (31)-(32)

IV. ESTIMATION OF MAGNETIC PARAMETERS

The seven parameters in the saturation model (7)-(8) must of course be estimated. This can be done with a rather simple procedure also relying on signal injection and averaging.

A. Principle

The rotor is locked in the position $\theta := 0$, hence the model (1)–(3) reduces to $\omega = 0$ and

$$\frac{d\phi_{dq}}{dt} = u_{dq} - Ri_{dq}, \quad (31)$$

with $i_{dq} = \mathcal{I}_{dq}(\phi_{dq})$. Moreover u_{dq} can now be physically impressed and i_{dq} physically measured.

As in section III-A, but now working directly in the $d-q$ frame, we inject a fast-varying pulsating voltage

$$u_{dq} = \bar{u}_{dq} + \tilde{u}_{dq}f(\Omega t), \quad (32)$$

with constant \bar{u}_{dq} and \tilde{u}_{dq} . The solution of (31)-(32) is then

$$\phi_{dq} = \bar{\phi}_{dq} + \frac{\tilde{u}_{dq}}{\Omega} F(\Omega t) + \mathcal{O}\left(\frac{1}{\Omega^2}\right)$$

TABLE I
RATED AND ESTIMATED MAGNETIC PARAMETERS OF TEST MOTORS

| Motor | IPM | SPM |
|--------------------------------|---------------|--------------|
| Rated power | 750 W | 1500 W |
| Rated current I_n (peak) | 4.51 A | 5.19 A |
| Rated voltage (peak per phase) | 110 V | 245 V |
| Rated speed | 1800 rpm | 3000 rpm |
| Rated torque | 3.98 Nm | 6.06 Nm |
| n | 3 | 5 |
| R | 1.52 Ω | 2.1 Ω |
| λ (peak) | 196 mWb | 155 mWb |
| L_d | 9.15 mH | 7.86 mH |
| L_q | 13.58 mH | 8.18 mH |
| $\alpha_{3,0}L_d^2I_n$ | 0.039 | 0.056 |
| $\alpha_{1,2}L_dL_qI_n$ | 0.053 | 0.055 |
| $\alpha_{4,0}L_d^3I_n^2$ | 0.0051 | 0.0164 |
| $\alpha_{2,2}L_dL_q^2I_n^2$ | 0.0171 | 0.027 |
| $\alpha_{0,4}L_q^3I_n^2$ | 0.0060 | 0.0067 |

where $\bar{\phi}_{dq}$, the ‘‘slowly-varying’’ component of ϕ_{dq} , satisfies

$$\frac{d\bar{\phi}_{dq}}{dt} = \bar{u}_d - R\bar{i}_d, \quad (33)$$

with $\bar{i}_{dq} = \mathcal{I}_{dq}(\bar{\phi}_{dq})$. Moreover (29) now boils down to

$$\tilde{i}_{dq} = D\mathcal{I}_{dq}(\mathcal{I}_{dq}^{-1}(\bar{i}_{dq}))\frac{\tilde{u}_{dq}}{\Omega}. \quad (34)$$

Since \bar{u}_{dq} is constant (33) implies $R\bar{i}_{dq}$ tends to \bar{u}_{dq} , hence after an initial transient \bar{i}_{dq} is constant. As a consequence \tilde{i}_{dq} is by (34) also constant. Fig. 1 shows for instance the time response of i_d for the SPM motor of section IV-C starting from $i_d(0) = 0$ and using a square function f ; notice the current ripples seen on the scope are $\max_{\tau \in [0, 2\pi]} F(\tau) = \frac{\pi}{2}$ (since f is square with period 2π) smaller than \tilde{i}_{dq} .

The magnetic parameters can then be estimated repeatedly using (34) with various values of \bar{u}_{dq} and \tilde{u}_{dq} , as detailed in the next section.

B. Estimation of the parameters

From (11) the entries of $D\mathcal{I}_{dq}(\mathcal{I}_{dq}^{-1}(\bar{i}_{dq}))$ are given by

$$G_{dd}(\bar{i}_{dq}) = \frac{1}{L_d} + 6\alpha_{3,0}L_d\bar{i}_d + 12\alpha_{4,0}L_d^2\bar{i}_d^2 + 2\alpha_{2,2}L_q^2\bar{i}_q^2$$

$$G_{dq}(\bar{i}_{dq}) = 2\alpha_{1,2}L_q\bar{i}_q + 4\alpha_{2,2}L_d\bar{i}_dL_q\bar{i}_q$$

$$G_{qq}(\bar{i}_{dq}) = \frac{1}{L_q} + 2\alpha_{1,2}L_d\bar{i}_d + 2\alpha_{2,2}L_d^2\bar{i}_d^2 + 12\alpha_{0,4}L_q^2\bar{i}_q^2.$$

Since combinations of the magnetic parameters always enter linearly those equations, they can be estimated by simple linear least squares; moreover by suitably choosing \bar{u}_{dq} and \tilde{u}_{dq} , the whole least squares problem for the seven parameters can be split into several subproblems involving fewer parameters:

- with $\bar{u}_{dq} := 0$, hence $\bar{i}_{dq} = 0$, (34) reads

$$L_d = \frac{1}{\Omega} \frac{\tilde{u}_d}{\tilde{i}_d} \quad (35)$$

$$L_q = \frac{1}{\Omega} \frac{\tilde{u}_q}{\tilde{i}_q} \quad (36)$$

- with $\bar{u}_q = 0$, hence $\bar{i}_q = 0$, and $\tilde{u}_q = 0$ (34) reads

$$\tilde{i}_d = \frac{\tilde{u}_d}{\Omega} \left(\frac{1}{L_d} + 6\alpha_{3,0}L_d\bar{i}_d + 12\alpha_{4,0}L_d^2\bar{i}_d^2 \right) \quad (37)$$

$$\tilde{i}_q = 0$$

- with $\bar{u}_d = 0$, hence $\bar{i}_d := 0$, and $\tilde{u}_q = 0$ (34) reads

$$\tilde{i}_d = \frac{\tilde{u}_d}{\Omega} \left(\frac{1}{L_d} + 2\alpha_{2,2}L_q^2\bar{i}_q^2 \right) \quad (38)$$

$$\tilde{i}_q = \frac{2\tilde{u}_d}{\Omega} \alpha_{1,2}L_q\bar{i}_q \quad (39)$$

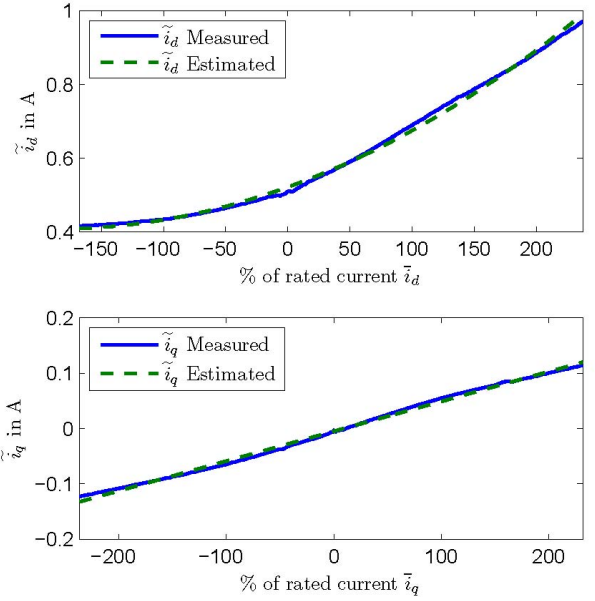


Fig. 2. IPM: fitted values vs measurements for (37) and (39)

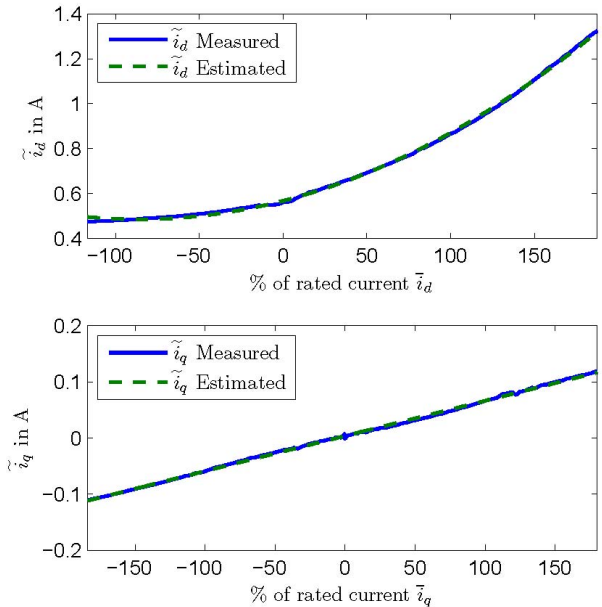


Fig. 3. SPM: fitted values vs measurements for (37) and (39)

- with $\bar{u}_d = 0$, hence $\bar{i}_d := 0$, and $\tilde{u}_d = 0$ (34) reads

$$\tilde{i}_d = \frac{2\tilde{u}_q}{\Omega} \alpha_{1,2} L_q \bar{i}_q \quad (40)$$

$$\tilde{i}_q = \frac{\tilde{u}_q}{\Omega} \left(\frac{1}{L_q} + 12\alpha_{0,4} L_q^2 \tau^2 \right). \quad (41)$$

L_d and L_q are then immediately determined from (35) and (36); $\alpha_{3,0}$ and $\alpha_{4,0}$ are jointly estimated by least squares from (37); $\alpha_{2,2}$, $\alpha_{1,2}$ and $\alpha_{0,4}$ are separately estimated by least squares from respectively (38), (39)-(40) and (41).

C. Experimental setup

The methodology developed in the paper was tested on two types of motors, an Interior Magnet PMSM (IPM) and a Surface-Mounted PMSM (SPM), with rated parameters listed in the top part of table I.

The experimental setup consists of an industrial inverter (400 V DC bus, 4 kHz PWM frequency), an incremental encoder, a dSpace fast prototyping system with 3 boards (DS1005, DS5202 and EV1048), and a host PC. The measurements

are sampled also at 4 kHz, and synchronized with the PWM frequency. The load torque is created by a 4 kW DC motor.

D. Estimation of the magnetic parameters

We follow the procedure described in section IV: with the rotor locked in the position $\theta := 0$, a square wave voltage with frequency $\Omega := 2\pi \times 500$ rad/s and constant amplitude \tilde{u}_d or \tilde{u}_q (15 V for the IPM, 14 V for the SPM) is applied to the motor; but for the determination of L_d, L_q where $\bar{u}_d = \bar{u}_q := 0$, several runs are performed with various \bar{u}_d (resp. \bar{u}_q) such that \bar{i}_d (resp. \bar{i}_q) ranges from -200% to $+200\%$ of the rated current. The magnetic parameters are then estimated by linear least squares according to section IV-B, yielding the values in the bottom part of table I. Notice the SPM exhibits as expected little geometric saliency ($L_d \approx L_q$) hence the saturation-induced saliency is paramount to estimate the rotor position. Notice also the cross-saturation term α_{12} is as expected quantitatively important for both motors.

The good agreement between the fitted curves and the measurements is demonstrated for instance for (37) and (39)

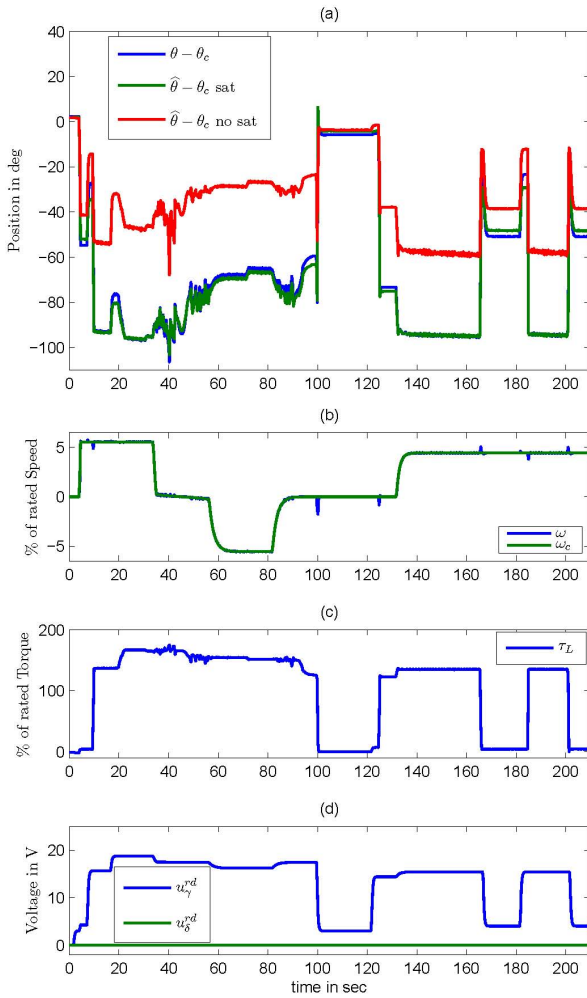


Fig. 4. Long test under various conditions for IPM: (a) measured $\theta - \theta_c$, estimated $\hat{\theta} - \theta_c$ with and without saturation model; (b) measured speed ω , reference speed ω_c ; (c) load torque τ_L ; (d) voltages $u_{\gamma\delta}^{rd}$

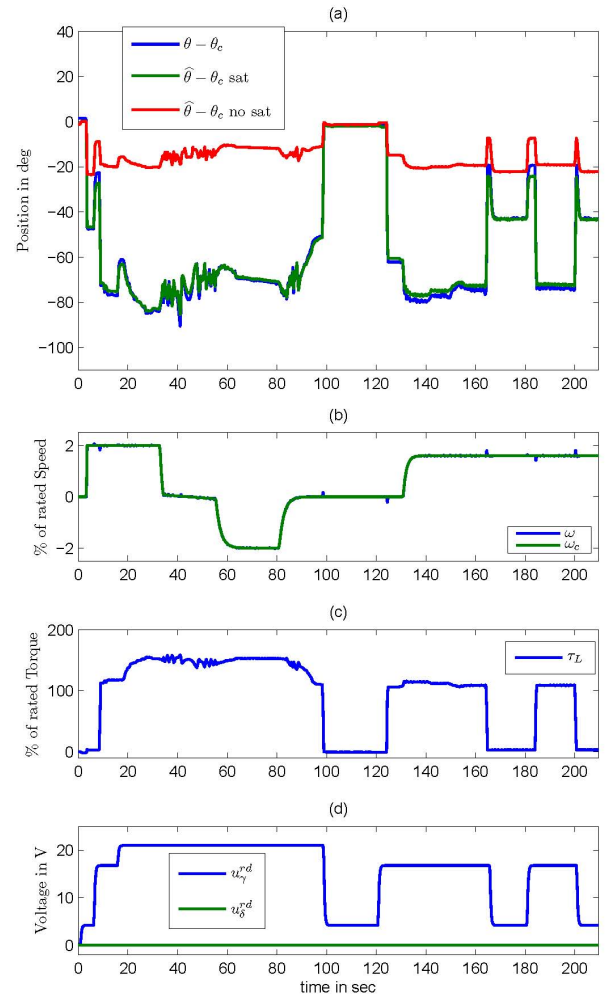


Fig. 5. Long test under various conditions for SPM: (a) measured $\theta - \theta_c$, estimated $\hat{\theta} - \theta_c$ with and without saturation model; (b) measured speed ω , reference speed ω_c ; (c) load torque τ_L ; (d) voltages $u_{\gamma\delta}^{rd}$

on Fig. 2-3; notice (37) corresponds to saturation on a single axis while (39) corresponds to cross-saturation.

E. Validation of the rotor position estimation procedure

The relevance of the position estimation methodology developed in section III is now illustrated on the two test motors, using the parameters estimated in the previous section. Since the goal is only to test the validity of the angle estimation procedure, a very simple V/f open-loop (i.e. Ω_c and $\mathcal{U}_{\gamma\delta}$ do not depend on $i_{\gamma\delta}$) control law is used for (12)–(16); a fast-varying ($\Omega := 2\pi \times 500$ rad/s) square voltage with constant amplitude is added in accordance with (21), resulting in

$$\begin{aligned} \frac{d\theta_c}{dt} &= \omega_c(t) \\ u_{\gamma\delta} &= u_{\gamma\delta}^d(t) + \omega_c(t)\phi_m + \tilde{u}_{\gamma\delta}f(\Omega t). \end{aligned}$$

Here $\omega_c(t)$ is the motor speed reference; $u_{\gamma\delta}^d(t)$ is a filtered piece-wise constant vector compensating the resistive voltage drop in order to maintain the torque level and the motor stability; finally $\tilde{u}_{\gamma\delta} := (\tilde{u}, 0)^T$ with $\tilde{u} := 15$ V.

The rotor position $\hat{\theta}$ is then estimated according to (30).

1) *Long test under various conditions, Fig. 4-5:* Speed and torque are changed over a period of 210 seconds; the speed remains between $\pm 5\%$ of the rated speed and the torque varies from 0% to 180% of the rated torque. This represents typical operation conditions at low speed.

When the saturation model is used the agreement between the estimated position $\hat{\theta}$ and the measured position θ is very good, with an error always smaller than a few (electrical) degrees. By contrast the estimated error without using the saturation model (i.e. with all the magnetic saturation parameters α_{ij} taken to zero) can reach up to 40° for the IPM and 70° for the SPM. This demonstrates the importance of considering an adequate saturation model including in particular cross-saturation.

2) *Slow speed reversal, Fig. 6-7:* This is an excerpt of the long experiment between 35 s and 55 s. The speed is slowly changed from -0.2% to $+0.2\%$ of the rated speed at 150% of the rated torque. This is a very demanding test since the motor always remains in the poor observability region, moreover under high load. Once again the estimated angle closely agrees with the measured angle.

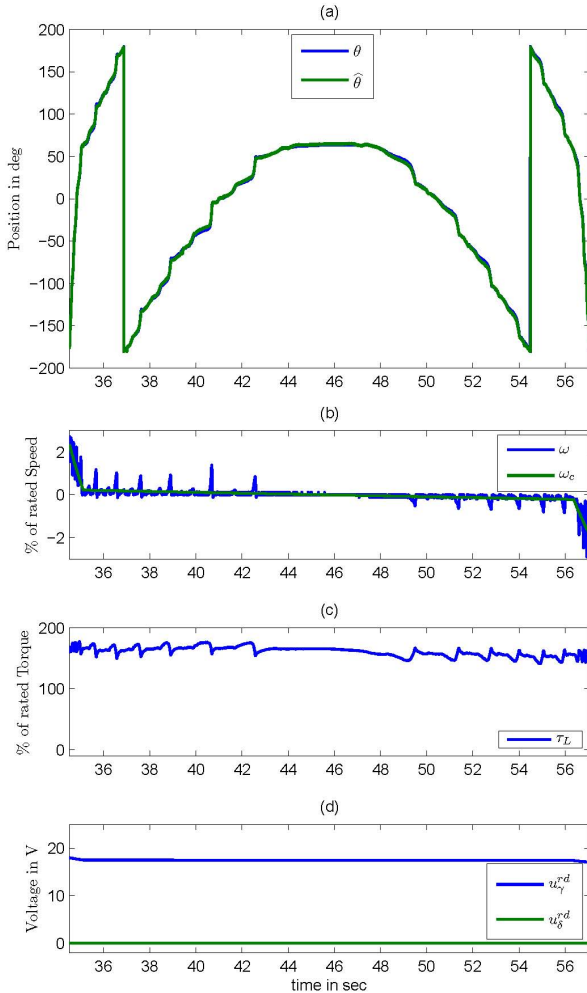


Fig. 6. Slow speed reversal for IPM: (a) measured θ , estimated $\hat{\theta}$; (b) measured speed ω , reference speed ω_c ; (c) load torque τ_L ; (d) voltages $u_{\gamma\delta}^d$

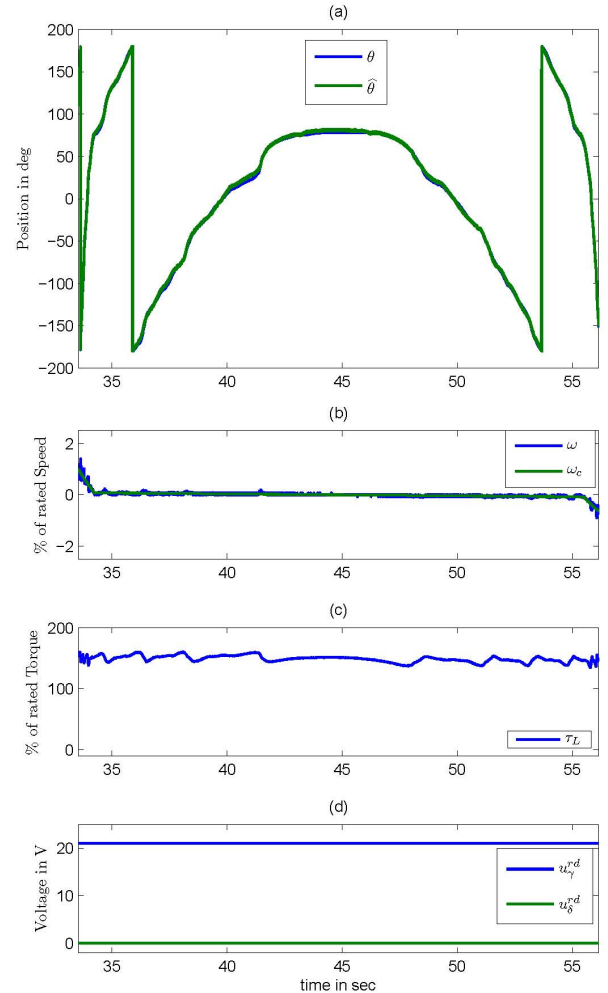


Fig. 7. Slow speed reversal for SPM: (a) measured θ , estimated $\hat{\theta}$; (b) measured speed ω , reference speed ω_c ; (c) load torque τ_L ; (d) voltages $u_{\gamma\delta}^d$

3) *Load step at zero speed, Fig. 8-9:* This is an excerpt of the long experiment around $t = 125$ s. The load is suddenly changed from 0% to 100% of the rated torque while the motor is at rest. This test illustrates the quality of the estimation also under dynamic conditions.

V. CONCLUSION

We have presented a simple parametric model of the saturated PMSM together with a new procedure based on signal injection for estimating the rotor angle at low speed relying on an original analysis based on second-order averaging. This is not an easy problem in view of the observability degeneracy at zero speed. The method is general in the sense it can accommodate virtually any control law, saturation model, and form of injected signal. The relevance of the method and the importance of using an adequate magnetic saturation model has been experimentally demonstrated on a SPM motor with little geometric saliency as well as on an IPM motor.

REFERENCES

[1] P. Jansen and R. Lorenz, "Transducerless position and velocity estimation in induction and salient AC machines," *IEEE Trans. Industry Applications*, vol. 31, pp. 240–247, 1995.

[2] S. Ogasawara and H. Akagi, "An approach to real-time position estimation at zero and low speed for a PM motor based on saliency," *IEEE Trans. Industry Applications*, vol. 34, pp. 163–168, 1998.

[3] M. Corley and R. Lorenz, "Rotor position and velocity estimation for a salient-pole permanent magnet synchronous machine at standstill and high speeds," *IEEE Trans. Industry Applications*, vol. 34, pp. 784–789, 1998.

[4] T. Aihara, A. Toba, T. Yanase, A. Mashimo, and K. Endo, "Sensorless torque control of salient-pole synchronous motor at zero-speed operation," *IEEE Trans. Power Electronics*, vol. 14, pp. 202–208, 1999.

[5] A. Consoli, G. Scarcella, and A. Testa, "Industry application of zero-speed sensorless control techniques for PM synchronous motors," *IEEE Trans. Industry Applications*, vol. 37, no. 2, pp. 513–521, 2001.

[6] J.-I. Ha, K. Ide, T. Sawa, and S.-K. Sul, "Sensorless rotor position estimation of an interior permanent-magnet motor from initial states," *IEEE Trans. Industry Applications*, vol. 39, no. 3, pp. 761–767, 2003.

[7] J.-H. Jang, S.-K. Sul, J.-I. Ha, K. Ide, and M. Sawamura, "Sensorless drive of surface-mounted permanent-magnet motor by high-frequency signal injection based on magnetic saliency," *IEEE Trans. Industry Applications*, vol. 39, pp. 1031–1039, 2003.

[8] J.-H. Jang, J.-I. Ha, M. Ohto, K. Ide, and S.-K. Sul, "Analysis of permanent-magnet machine for sensorless control based on high-frequency signal injection," *IEEE Trans. Industry Applications*, vol. 40, no. 6, pp. 1595–1604, 2004.

[9] E. Robeischl and M. Schroedl, "Optimized INFORM measurement sequence for sensorless PM synchronous motor drives with respect to minimum current distortion," *IEEE Trans. Industry Applications*, vol. 40, no. 2, pp. 591–598, 2004.

[10] S. Shinnaka, "A new speed-varying ellipse voltage injection method for

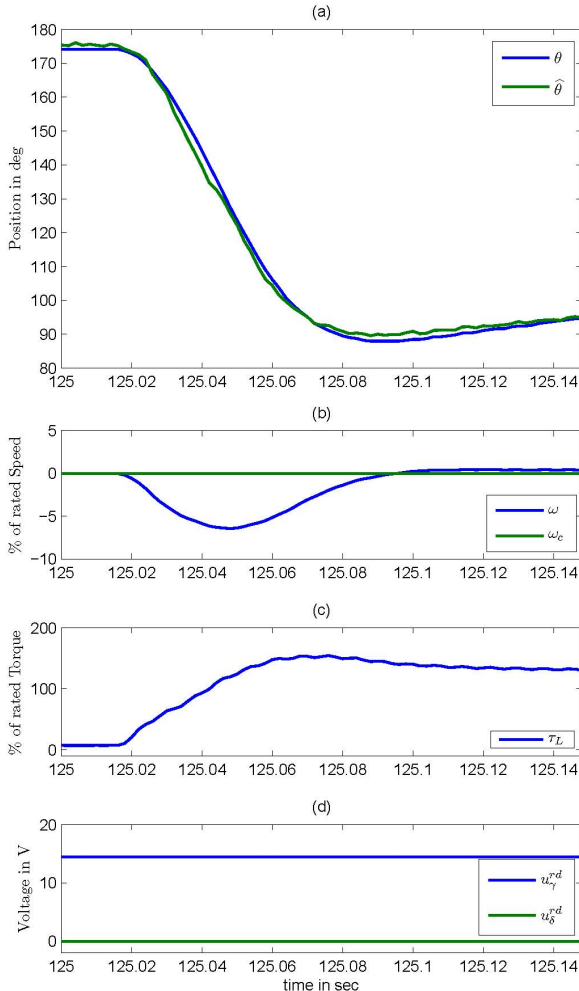


Fig. 8. Load step at zero speed for IPM: (a) measured θ , estimated $\hat{\theta}$; (b) measured speed ω , reference speed ω_c ; (c) load torque τ_L ; (d) voltages $u_{\gamma}^{r,d}$

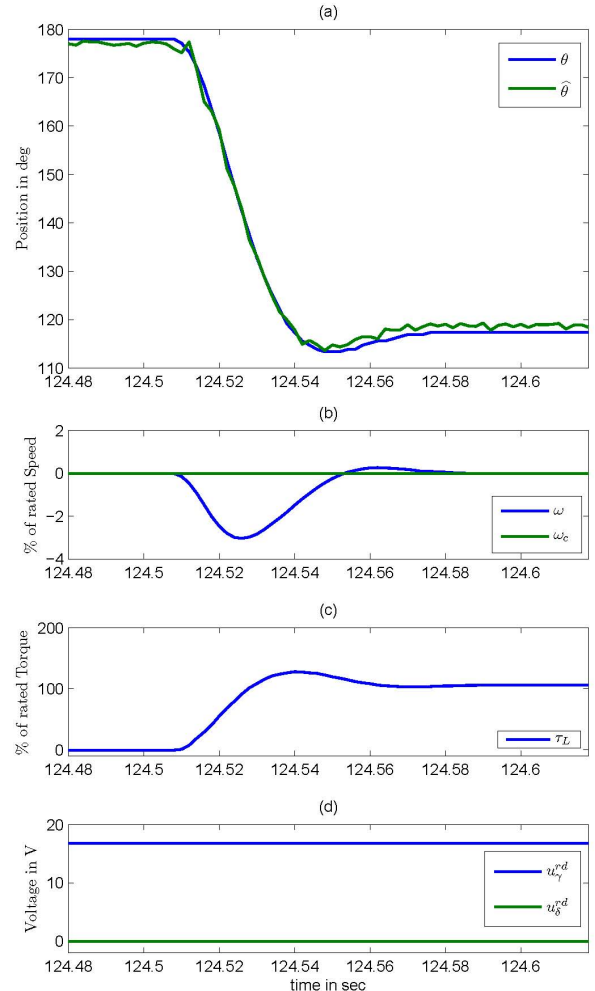


Fig. 9. Load step at zero speed for SPM: (a) measured θ , estimated $\hat{\theta}$; (b) measured speed ω , reference speed ω_c ; (c) load torque τ_L ; (d) voltages $u_{\gamma}^{r,d}$

- sensorless drive of permanent-magnet synchronous motors with pole saliency - New PLL method using high-frequency current component multiplied signal," *IEEE Trans. Industry Applications*, vol. 44, no. 3, pp. 777–788, 2008.
- [11] L. Harnefors and H.-P. Nee, "A general algorithm for speed and position estimation of AC motors," *IEEE Trans. Industrial Electronics*, vol. 47, no. 1, pp. 77–83, 2000.
- [12] O. Wallmark, L. Harnefors, and O. Carlson, "An improved speed and position estimator for salient permanent-magnet synchronous motors," *IEEE Trans. Industrial Electronics*, vol. 52, no. 1, pp. 255–262, 2005.
- [13] C. Silva, G. Asher, and M. Sumner, "Hybrid rotor position observer for wide speed-range sensorless PM motor drives including zero speed," *IEEE Trans. Industrial Electronics*, vol. 53, no. 2, pp. 373–378, 2006.
- [14] A. Piippo, M. Hinkkanen, and J. Luomi, "Analysis of an adaptive observer for sensorless control of interior permanent magnet synchronous motors," *IEEE Trans. Industrial Electronics*, vol. 55, no. 2, pp. 570–576, 2008.
- [15] G. Foo and M. Rahman, "Sensorless sliding-mode MTPA control of an IPM synchronous motor drive using a sliding-mode observer and HF signal injection," *IEEE Trans. Industrial Electronics*, vol. 57, no. 4, pp. 1270–1278, 2010.
- [16] P. Guglielmi, M. Pastorelli, and A. Vagati, "Cross-saturation effects in IPM motors and related impact on sensorless control," *IEEE Trans. Industry Applications*, vol. 42, pp. 1516–1522, 2006.
- [17] N. Bianchi, S. Bolognani, J.-H. Jang, and S.-K. Sul, "Comparison of PM motor structures and sensorless control techniques for zero-speed rotor position detection," *IEEE Trans. Power Electronics*, vol. 22, no. 6, pp. 2466–2475, 2007.
- [18] J. Holtz, "Acquisition of position error and magnet polarity for sensorless control of PM synchronous machines," *IEEE Trans. Industry Applications*, vol. 44, no. 4, pp. 1172–1180, 2008.
- [19] D. Reigosa, P. García, D. Raca, F. Briz, and R. Lorenz, "Measurement and adaptive decoupling of cross-saturation effects and secondary saliencies in sensorless controlled IPM synchronous machines," *IEEE Trans. Industry Applications*, vol. 44, no. 6, pp. 1758–1767, 2008.
- [20] N. Bianchi, S. Bolognani, and A. Faggion, "Predicted and measured errors in estimating rotor position by signal injection for salient-pole PM synchronous motors," in *IEEE International Electric Machines and Drives Conference*, 2009, pp. 1565–1572.
- [21] H. De Kock, M. Kamper, and R. Kennel, "Anisotropy comparison of reluctance and PM synchronous machines for position sensorless control using HF carrier injection," *IEEE Trans. Power Electronics*, vol. 24, no. 8, pp. 1905–1913, 2009.
- [22] Y. Li, Z. Zhu, D. Howe, C. Bingham, and D. Stone, "Improved rotor-position estimation by signal injection in brushless AC motors, accounting for cross-coupling magnetic saturation," *IEEE Trans. Industry Applications*, vol. 45, pp. 1843–1850, 2009.
- [23] P. Sergeant, F. De Belie, and J. Melkebeek, "Effect of rotor geometry and magnetic saturation in sensorless control of PM synchronous machines," *IEEE Trans. Magnetics*, vol. 45, no. 3, pp. 1756–1759, 2009.
- [24] D. Raca, P. García, D. Reigosa, F. Briz, and R. Lorenz, "Carrier-signal selection for sensorless control of PM synchronous machines at zero and very low speeds," *IEEE Trans. Industry Applications*, vol. 46, no. 1, pp. 167–178, 2010.
- [25] N. Bianchi, E. Fornasiero, and S. Bolognani, "Effect of stator and rotor saturation on sensorless rotor position detection," in *IEEE Energy Conversion Congress and Exposition*, 2011, pp. 1528–1535.
- [26] Z. Zhu and L. Gong, "Investigation of effectiveness of sensorless operation in carrier-signal-injection-based sensorless-control methods," *IEEE Trans. Industrial Electronics*, vol. 58, no. 8, pp. 3431–3439, 2011.
- [27] F. Parasiliti and P. Poffet, "Model for saturation effects in high-field permanent magnet synchronous motors," *IEEE Trans. Energy Conversion*, vol. 4, no. 3, pp. 487–494, 1989.
- [28] M. Cheng, K. Chau, and C. Chan, "Nonlinear varying-network magnetic circuit analysis for doubly salient permanent-magnet motors," *IEEE Trans. Magnetics*, vol. 36, no. 1 PART 2, pp. 339–348, 2000.
- [29] B. Štumberger, G. Štumberger, D. Dolinar, A. Hamler, and M. Trlep, "Evaluation of saturation and cross-magnetization effects in interior permanent-magnet synchronous motor," *IEEE Trans. Industry Applications*, vol. 39, no. 5, pp. 1264–1271, 2003.
- [30] K. Rahman and S. Hiti, "Identification of machine parameters of a synchronous motor," *IEEE Trans. Industry Applications*, vol. 41, no. 2, pp. 557–565, 2005.
- [31] G. Štumberger, B. Štumberger, B. Štumberger, M. Toman, and D. Dolinar, "Evaluation of experimental methods for determining the magnetically nonlinear characteristics of electromagnetic devices," *IEEE Trans. Magnetics*, vol. 41, no. 10, pp. 4030–4032, 2005.
- [32] E. Armando, P. Guglielmi, G. Pellegrino, M. Pastorelli, and A. Vagati, "Accurate modeling and performance analysis of IPM-PMASR motors," *IEEE Trans. Industry Applications*, vol. 45, no. 1, pp. 123–130, 2009.
- [33] A. Jebai, F. Malrait, P. Martin, and P. Rouchon, "Estimation of saturation of permanent-magnet synchronous motors through an energy-based model," in *IEEE International Electric Machines Drives Conference*, 2011, pp. 1316–1321.
- [34] Y.-D. Yoon, S.-K. Sul, S. Morimoto, and K. Ide, "High-bandwidth sensorless algorithm for AC machines based on square-wave-type voltage injection," *IEEE Trans. Industry Applications*, vol. 47, no. 3, pp. 1361–1370, 2011.
- [35] D. Basic, F. Malrait, and P. Rouchon, "Euler-Lagrange models with complex currents of three-phase electrical machines and observability issues," *IEEE Trans. Automatic Control*, vol. 55, pp. 212–217, 2010.
- [36] D. Basic, A. K. Jebai, F. Malrait, P. Martin, and P. Rouchon, "Using Hamiltonians to model saturation in space vector representations of AC electrical machines," in *Advances in the theory of control, signals and systems with physical modeling*, ser. Lecture Notes in Control and Information Sciences, J. Lévine and P. Müllhaupt, Eds. Springer, 2011, pp. 41–48.
- [37] J. A. Sanders, F. Verhulst, and J. Murdock, *Averaging methods in nonlinear dynamical systems*, 2nd ed., ser. Applied Mathematical Sciences. Springer, 2007, no. 59.